Pure Appl. Chem., Vol. 80, No. 11, pp. 2297–2308, 2008.
doi:10.1351/pac200880112297
© 2008 IUPAC

Single-chain magnets constructed with a twisting arrangement of the easy-plane of iron(II) ions*

Takashi Kajiwara‡, Hiroki Tanaka, and Masahiro Yamashita

Graduate School of Science, Tohoku University and JST, Aza-aoba, Aramaki, Aoba-ku, Sendai 980-8578, Japan

Abstract: A novel class of single-chain magnets (SCMs), *catena*-$[Fe^{II}(ClO_4)_2\{Fe^{III}(bpca)_2\}]ClO_4$ and its derivative, were synthesized using the spin-carrier components possessing hard-axis anisotropy (or easy-plane anisotropy, $D > 0$). The easy-axis-type anisotropy of whole molecules of these compounds, which is essential for the formation of SCMs, arises from the twisted arrangement of easy-planes of Fe(II) along the chain axis. Alternating high-spin Fe(II) and low-spin Fe(III) chain complexes behave as an SCM with a typical frequency-dependent ac susceptibility which obeys Arrhenius law. Below 7 K, *catena*-$[Fe^{II}(ClO_4)_2\{Fe^{III}(bpca)_2\}]ClO_4$ showed a short-range spin-ordering even in zero external field in a time range of Mössbauer spectroscopy as well as the muon-spin-relaxation (μSR) spectroscopy. Since the easy-axis-type magnetic anisotropy originated from the structural motif of the twisting arrangement of Fe(II) ions, the overall magnetic property was very sensitive to the small structural changes arising from adsorption/desorption of the crystal solvents, and *catena*-$[Fe^{II}(ClO_4)_2\{Fe^{III}(bpca)_2\}]ClO_4$ showed a reversible change in magnetism that has been referred to as "a magnetic sponge". In its derivative, controls of the molecular structure, the arrangement of chains in the crystal, and magnetic properties both in dc and ac susceptibility have been achieved by the introduction of methyl group on a $bpca^-$ ligand, which bridges and mediates the magnetic interaction of the adjoining Fe(II)/Fe(III) ions.

Keywords: single-chain magnets; iron; metal complex; magnetism; Mössbauer spectrum; muon-spin-relaxation spectrum.

INTRODUCTION

Using bottom-up approaches, metal-assembled complexes have been constructed with new structural motifs, properties, and functionalities. Single-molecule magnets (SMMs) and single-chain magnets (SCMs) are among the most important classes of complexes constructed by bottom-up approaches, since they show unique physical properties [1–3] that are not observed in bulk magnets. These magnets are considered candidates for molecular electronics and high-density memory devices because of their size and the facility with which their shape and properties can be controlled. The molecular nanomagnets, including SMMs and SCMs, have well-defined structures and exhibit well-characterized easy-axis magnetic anisotropy (Fig. 1, $D < 0$). When the high-spin molecules with the total spin of S have easy-axis-type magnetic anisotropy, their sublevels of the ground spin state divide to form a "double-

*Paper based on a presentation at the 3rd International Symposium on Novel Materials and Their Synthesis (NMS-III) and the 17th International Symposium on Fine Chemistry and Functional Polymers (FCFP-XVII), 17–21 October 2007, Shanghai, China. Other presentations are published in this issue, pp. 2231–2563.

‡Corresponding author: E-mail: kajiwara@agnus.chem.tohoku.ac.jp

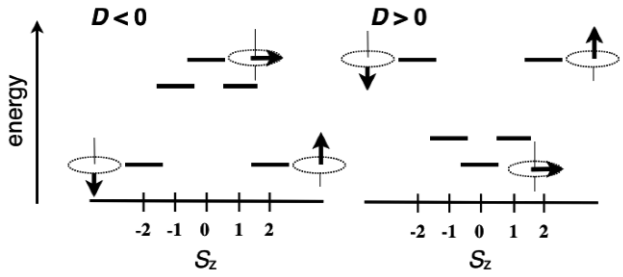

Fig. 1 Schematic representation of the magnetic anisotropy for the case of $S = 2$, such as high-spin Fe(II) ion. The energy of the each sublevel is defined as $D|S_z|^2$.

well potential" with the depth of $|D|S^2$. The resultant energy barrier is sufficiently large at low temperature to prevent the reversal of the spin flipping, and each molecule behaves as a magnet in this low-temperature range. The first SMM is the famous mixed-valent dodeca-manganese cluster $[Mn_{12}O_{12}(OAc)_{16}(H_2O)_4]$, which possesses a uni-axial anisotropy (or negative D) which arose from a spatial alignment of anisotropy axes of peripheral Mn(III) ions [1–4]. After the finding of the first SMM, several types of SMM were reported in which the magnetic anisotropy of the whole molecules originated mainly from metal ions possessing negative D such as Mn(III), Co(II) [5,6], and heavy lanthanide ions such as Tb(III) [7] and Dy(III) [8]. SCMs form another important class of the nanomagnets consisting of alternating magnetic components such as a nitronyl nitroxide radical/Co^{2+} [9], Mn^{3+}/Ni^{2+} [10], Fe^{3+}/Co^{2+} [11], and so on [12], to form 1D Ising-type chain. In these cases, the magnetic anisotropy of the whole chain arises from the ions with easy-axis anisotropy such as Mn(III), Co(II), and Dy(III), and it can be concluded that the usage of easy-axis-type metal ions is advantageous for consistent nanomagnets.

In 2000, H. Oshio et al. reported a new strategy for syntheses of SMMs employing Fe(II) ions as a anisotropy source, which possesses a hard-axis-type anisotropy, or easy-plane anisotropy (Fig. 1, $D > 0$) [13,14]. The overall easy-axis anisotropy of the molecule arises from the orthogonal arrangement of easy-planes of each Fe(II) ion. The new concept for construction of an SMM using metal ions with positive D was summarized by H. Oshio and M. Nakano [15]. Along with the same concept, we succeeded in constructing a novel SCM of which the molecular anisotropy arises from the twisting arrangement of easy-planes of high-spin Fe(II) ions [16]. The chain complex was obtained by the alternating arrangement of low-spin Fe(III) and high-spin Fe(II) ions. The easy-plane spins are coupled through the nearly isotropic Fe(III) $S = 1/2$ spins in a ferrimagnetic manner, forming a unique XY spin chain with twisting of the axis of anisotropy. In this review, we will summarize the magnetism of the new SCMs of Fe(III)–Fe(II) alternate chains, as well as the unique properties of the SCM, arising from the strong correlation between molecular structures and magnetism.

STRUCTURES AND MAGNETISM

A systematic synthetic method has been developed for preparation of homo- and hetero-metal chain systems using mononuclear complexes $\{M(bpca)_2\}$ [17–19] and $\{M'(bpca)_2\}^+$ [20,21] ($M = Mn^{II}$, Fe^{II}, Ni^{II}; $M' = Cr^{III}$, Fe^{III}, Co^{III}; Hbpca = bis(2-pyridylcarbonyl)amine). X-ray analyses of $\{M(bpca)_2\}^{0/+}$ revealed that two $bpca^-$ ligands are orthogonally arranged around the metal ion behaving as a *facial* N_3 ligand, and they generate a strong ligand field that constrains the metal ion to adopt a low-spin state. The mononuclear complexes could potentially behave as a bis-bidentate ligand via two sets of two carbonyl oxygen atoms directing the opposite sides, and we have synthesized several structural motives including zero-dimensional trinuclear complexes, one-dimensional chain complexes, and two-dimensional honeycomb-layered complexes, by controlling the reaction conditions. The reaction of Fe(II)

ions and $\{M^{III}(bpca)_2\}^+$ involving trivalent M of Fe, Cr, or Co resulted to form isostructural chain complexes of *catena*-$[Fe^{II}(ClO_4)_2\{M^{III}(bpca)_2\}]ClO_4$ [M = Fe (**1**), Cr (**2**), Co (**3**)], and their magnetic behavior was investigated by means of dc susceptibility measurements. In these complexes, the ferrimagnetic Fe(II)–Fe(III) complex showed an abrupt increase of $\chi_M T$ values at low temperature, which could be related to the occurrence of spin-ordering, and the further detail of the magnetism was examined to confirm the potential as an SCM.

The X-ray analysis revealed that the chain lies along a crystallographic *a*–*c* vector, and the crystals grow along this axis. The shortest intra- and interchain Fe**…**Fe distances are estimated to be 5.178 Å and longer than 10 Å, respectively, and interchain interactions are considered to be negligible.

The Fe(III) ions (represented as gray spheres in Fig. 2) are located in a slightly compressed octahedron along the chain axis, whereas the Fe(II) ions (black spheres) have an axially elongated geometry with four equatorial carbonyl oxygen atoms [2.0275(14)–2.0659(13) Å] and two axial ClO_4^- oxygen atoms [2.1208(14) and 2.1516(14) Å]. In this coordination environment, the $S = 2$ spin on the Fe(II) ions is considered to have a hard-axis-type anisotropy along the O_{ax}–Fe–O_{ax} axis, or easy-plane-type anisotropy in the equatorial plane involving four $O_{carbonyl}$ atoms. The Mössbauer spectrum was measured to confirm the oxidation states and spin states of these sites at ambient temperature. It was found that the Fe(III) ion takes a low-spin state with the isomer shift δ and the quadrupole splitting ΔE_Q of 1.15 and 0.03 mm s^{-1}, respectively, whereas the Fe(II) ion takes a high-spin state with the Mössbauer parameters of 2.49 and 0.41 mm s^{-1}, all of the parameters being in typical values for these oxidation and spin states.

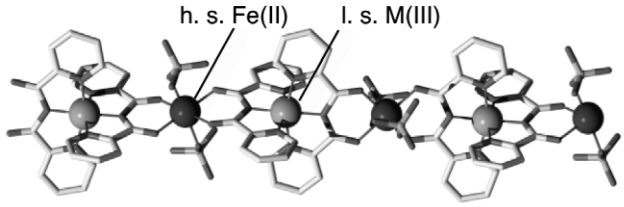

Fig. 2 Crystal structures of cationic part of *catena*-$[Fe^{II}(ClO_4)_2\{M^{III}(bpca)_2\}]ClO_4$.

The field dependence of the magnetization was measured for the single crystal with a magnetic field applied parallel or perpendicular to the chain. A rapid increase and saturation of the magnetization was observed in the dc field parallel to the chain, however, a gradual increase of the magnetization was observed in the field perpendicular to the chain which did not saturate until 50 kOe. The result indicates that **1** possesses an easy axis along the chain. An anisotropy of the susceptibility was also observed for the single-crystal sample (Fig. 3, right), which was analyzed on the basis of the spin Hamiltonian considering the super-exchange interaction between neighboring Fe(II) and Fe(III) ions, J, and the uni-axial zero-field splitting parameter for each Fe(II) spin, D. The parameters J/k_B and D/k_B were estimated to be –10.0 and 14.9 K, respectively. Although the magnetization study suggests the presence of an easy-axis-type anisotropy for the entire crystal, the single-site anisotropy D is of an easy-plane type, the latter is consistent with the structural description.

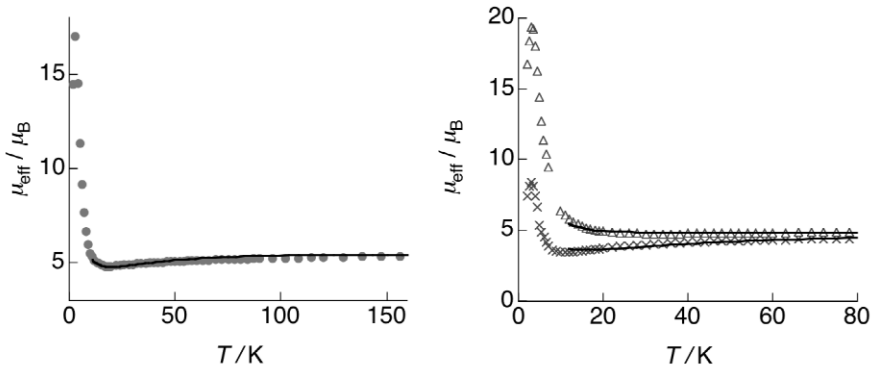

Fig. 3 (Left) Temperature dependence of μ_{eff} for the powder sample. (Right) Dc susceptibility measurements on an oriented single crystal of **1** in the magnetic field applied along the chain (Δ) and perpendicular to the chain (x). The solid lines are theoretical curves.

To clarify the possibility that **1** is an SCM, ac magnetic susceptibility measurements were performed with a powder sample to observe the frequency dependence of χ_M" signals (Fig. 4). As the frequency was swept from 5 to 1000 Hz, the temperature of maximum of χ_M" shifted from 1.8 to 2.6 K. At fixed temperatures between 2.0 and 2.6 K, semicircle Cole–Cole plots were obtained with small α parameters in the range of 0.09–0.13, which indicates that relaxation occurs via a single process [4,22,23].

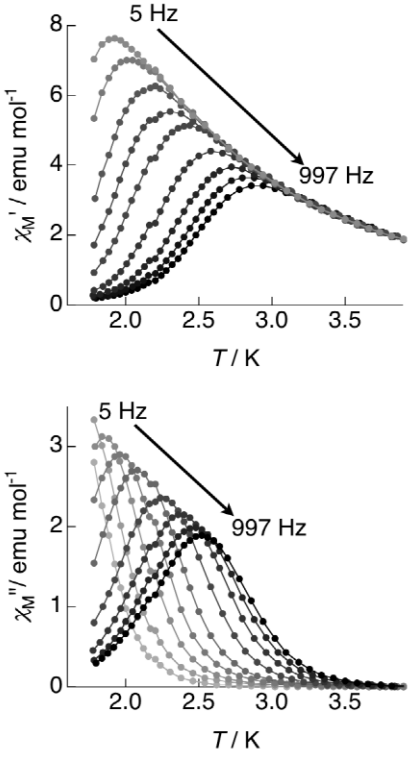

Fig. 4 In-phase (top, χ_M') and out-of-phase (bottom, χ_M") ac magnetic susceptibility vs. temperature in a 3.0 Oe ac field oscillating at the indicated frequencies and with a zero dc field.

The typical SCM behavior shown here should be attributed to a mutually orthogonal arrangement of the Fe(II) molecular axes inducing Ising interactions along the chain (Scheme 1).

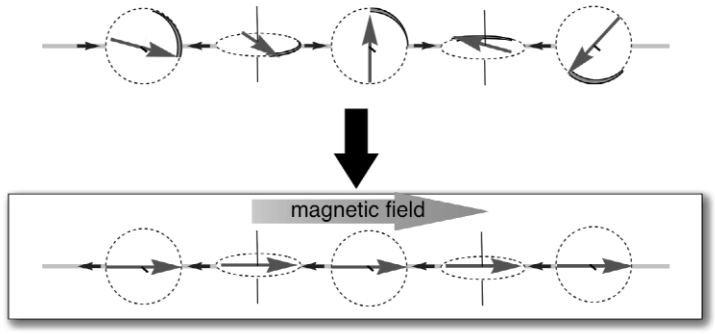

Scheme 1

It is likely that the large easy-plane anisotropies of the Fe(II) ions are added together, noting the mutual orthogonality of the quantization axes, to afford a net easy-axis anisotropy along the chain. The relaxation times $\tau(T)$ extracted from the ac susceptibility and Mössbauer data were used to construct an Arrhenius plot, giving an estimated activation energy Δ/k_B of 27(1) K. This Δ/k_B value is smaller than the $8J + |D|S^2$ expected for pure Glauber's dynamics [24,25], suggesting that the transverse magnetization of the Fe(II) spins in an easy plane is responsible for the magnetic relaxation. This twisting easy-plane system is unique in that it exhibits easy-axis anisotropy over the whole chain, giving rise to slow magnetization reversal despite single-ion anisotropy of the constituent Fe(II) ions with easy-plane.

SHORT-RANGE SPIN-ORDERING IN ZERO EXTERNAL MAGNETIC FIELD

A short-range spin-ordering of **1** in zero external field has been observed by temperature-dependent Mössbauer spectroscopy as well as muon-spin-relaxation (μSR) spectroscopy (Fig. 5) [26].

The Mössbauer spectra were measured down to 3.7 K in zero external field. Two sets of doublet signals were observed down to 20 K, which were assigned to high-spin Fe(II) and low-spin Fe(III) ions, respectively. Broadening due to a paramagnetic relaxation occurred below 7 K, and two sets of sextet signals appeared at 3.7 K, where the spin reversal slows down below the Mössbauer timescale of 10^{-7} s. Even at 3.7 K, the spectrum shows very broad signal, indicating the absence of long-range spin-ordering. The spectrum was roughly simulated with the overlapping of two ordered signals with six peaked of each Fe(II) and F(III) ions as well as a small portion of two paramagnetic signals. From the simulation spectrum, it was estimated that the Fe nuclei feel quasi-static hyperfine fields H_n of 192 kOe for Fe(II) and 335 kOe for Fe(III), respectively.

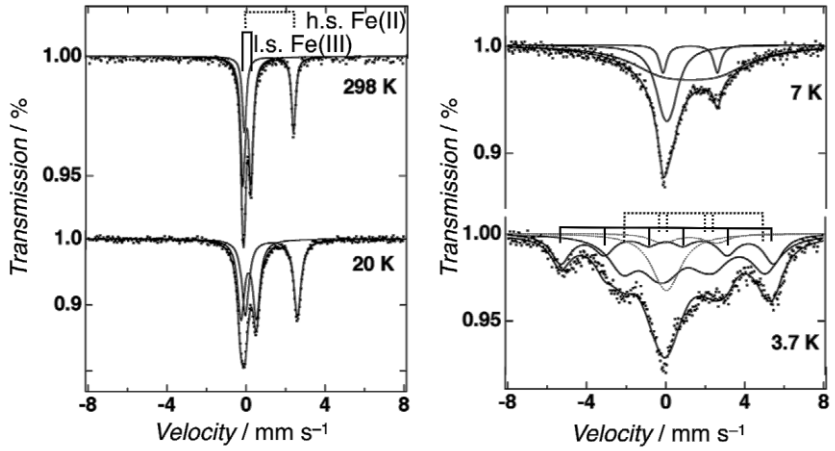

Fig. 5 Temperature dependence of the ^{57}Fe Mössbauer spectra of **1**.

μSR is a unique experimental method to sense the fluctuation of weak magnetic fields formed within the characteristic time window of 10^{-6}–10^{-11} s, which covers the Mössbauer timescale of 10^{-7} s. Because the muon has a half spin with the large gyromagnetic ratio ($\gamma_\mu = 2\pi \times 13.55$ MHz/kOe), which is four times larger than that of the proton, μSR is a highly sensitive and powerful probe of the solid-state magnetic materials [27–32]. Making use of the self-polarization of the muon spin, the growth of a spin-ordering of Fe(II) spins can be probed even in the zero-field condition. Forward and backward counters were located on the upstream and downstream sides in the beam direction, which was parallel to the initial muon-spin direction. Injected muons lose their energy and stop at the minimum of the Coulomb potential, then the stopped muons decay with a lifetime of 2.2 μs and emit positrons preferentially along the spin direction (Fig. 6). These positrons were detected to obtain the asymmetry parameter $A(t)$, defined as $A(t) = [F(t) - B(t)]/[F(t) + B(t)]$, with $F(t)$ and $B(t)$ denoting the numbers of positrons counted by the forward and backward counters at t. When the muon is placed in a uniform magnetic field, all the stopped muon spins precess at the same frequency to give a Larmor precession of the asymmetry. The presence of the precession on the time spectrum indicates formation of a long-range, spin-ordered state.

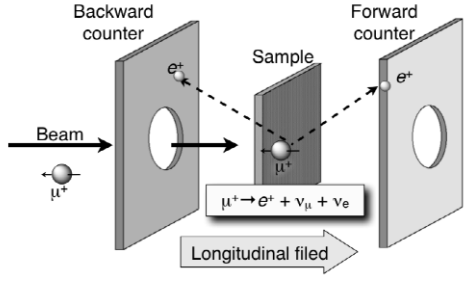

Fig 6 Schematic drawing of the μSR measurement equipment.

The time spectra (Fig. 7) show Gaussian-type depolarization behavior above 6 K. The initial asymmetry $A(0)$ decreases as the temperature is lowered, and this indicates that the slowing down of the Fe spin fluctuation starts at low temperature to be observable by μSR. The absence of precession even at 0.3 K indicates that the muon is located in a randomly distributed magnetic field, in conformity with the growth of short-range ordering of Fe(II) ions observed by Mössbauer spectra in the same tempera-

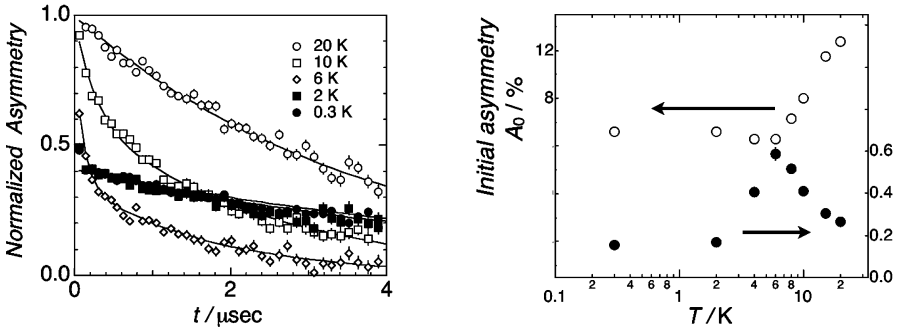

Fig. 7 (Left) Zero-field μSR time spectra of the complex **1** at various temperatures. Solid lines are the best fit results using single- or double-exponential functions. (Right) Temperature dependence of the initial asymmetry of the slow depolarizing component (A_0) and the depolarization rate (λ_0).

ture range. At low temperatures below 6 K, the asymmetry of the muon-spin polarization decreases quickly by nearly two-thirds, within a time range of 0.5 μs after the arrival of muons in the sample. The remaining one-third of the asymmetry depolarized slowly thereafter.

The time spectra were analyzed using the single exponential expression of $A_0\exp(-\lambda_0 t)$ (at 20 K) or two-exponential function of $A_0\exp(-\lambda_0 t) + A_1\exp(-\lambda_1 t)$ (below 20 K), where λ_0 and λ_1 are the depolarization rates and A_0 and A_1 are the initial asymmetries. The initial asymmetry A_0 decreases with decreasing temperature, reaches a minimum at 6 K, and assumes a constant value below 2 K (Fig. 7 right). The λ_0 is enhanced with decreasing temperature and exhibits divergence at 6 K. These are typical characteristics for the appearance of a static magnetically ordered state below 6 K, which correlates with the appearance of a paramagnetic relaxation below 7 K observed by Mössbauer spectroscopy. The lack of the observation of coherent muon-spin precession in the magnetically ordered state below 6 K implies that muons are probably located in a widely distributed magnetic field. This result supports the picture of the short-range ordered Fe(II) ions observed by Mössbauer spectra in the same temperature range. Because of the short-range ordering of Fe(II) ions, the muon-spin polarization decays owing to distributed precession frequencies, and the amplitude of the asymmetry decreases with time.

Within the characteristic time windows of Mössbauer and μSR, the uni-axial anisotropy arising from the twisted arrangement of easy-plane anisotropy resulted in a slow reversal of the spin even in a zero-external field below 7–6 K.

SOLVENT-INDUCED REVERSIBILTY OF MAGNETISM OF 1

One of the major advantages of molecular-based magnets is their controllability in structures, which allows fine-tuning of magnetic behavior. With this advantage, a lot of designed molecular magnetic materials are reported, of which the magnetic properties can be controlled by some external stimulus [33,34]. "Magnetic sponges" are one such class [35–37]. A magnetic sponge can release or reabsorb solvent molecules in a reversible manner like "sponges", which is accompanied by a drastic change of magnetic properties. As described in the previous sections, the easy-axis anisotropy of **1** resulted from the spatial arrangement of the hard axis of the Fe(II) ions, and hence the magnetism of **1** could be very sensitive to the small structural changes [38].

Compound **1** crystallizes in the monoclinic crystal system with the space group $P2_1/n$, with the formula of $\mathbf{1}\cdot 3CH_3NO_2$. The CH_3NO_2 molecules are released gradually at room temperature, and the crystal disintegrates. Thermogravimetric analysis for the fresh crystals of **1** was carried out to show 19 % decrease of weight at 30 °C, which corresponds to the loss of three CH_3NO_2 molecules from the solvated crystal. Hereafter, we refer to the crystal which contains three CH_3NO_2 molecules as the *sol-*

vated sample (**1**·3CH_3NO_2), and the crystal which has released all CH_3NO_2 molecules as the *dried* sample (**1**).

Since the completely dried sample **1** does not maintain the quality for the single-crystal X-ray diffraction, structure analysis was first carried out on a partially dried sample, **1**·2.5CH_3NO_2, which maintains enough quality for the data correction. **1**·2.5CH_3NO_2 has a similar structure to that of **1**·3CH_3NO_2, however, the space group changes from $P2_1/n$ to $C2/c$, with the unit cell volume decreases from 3966 to 3910 Å^3. Intra- and interchain Fe–Fe distances are maintained during this change of volume. X-ray powder diffraction (XRD) patterns were analyzed for the completely dried **1**, which keeps the crystal character in this condition and does not change to the amorphous phase. The XRD patterns of **1** were similar to those of **1**·2.5CH_3NO_2, and a Rietvelt analysis was performed for **1** on the basis of X-ray data of **1**·2.5CH_3NO_2 with space groups of $C2/c$. The resulting unit cell volume of 3815 Å^3 is consistent with the complete loss of solvent molecules.

Interestingly, a dried sample reabsorbs CH_3NO_2 and restores the original condition of the solvated sample. The completely dried sample assimilated CH_3NO_2, which resulted in an XRD very similar to the simulation XRD pattern obtained from data of the single crystal. The Rietvelt analysis shows the reversion of unit cell volume to 4039 Å^3, which indicates that the dried crystal reabsorbs CH_3NO_2 molecules and reverts to the solvated condition. The crystal of complex **1** can release or reabsorb CH_3NO_2 molecules reversibly like "sponges", possessing the chain structure of **1**.

The magnetic behavior of these two samples are different both in dc and ac susceptibilities. Under 20 K, the $\chi_M T$ value of dried sample rapidly increased to a maximum value of 58.7 emu K mol^{-1} around 3 K, on the other hand, the $\chi_M T$ value of solvated sample starts increasing at lower temperature (13 K) and does not show a peak down to 1.8 K (Fig. 8, upper). A similar trend was observed in the frequency dependence of the out-of-phase ac magnetic susceptibility (χ_M") of the solvated and dried samples (Fig. 8, bottom). With the crystal condition changed from the solvated to the dried, the peak top at which χ_M" has the maximum value shifts toward higher temperature. From the analysis using the Arrhenius equation, values of Δ/k_B were estimated as 21.9(3) K for the solvated condition, and 26.0(9) K for the dried condition, respectively. Δ/k_B increases when the crystal state changes from the solvated condition to the dried condition. α values both for the solvated and dried samples estimated from the Cole–Cole plots were small enough (0.24 and 0.14, respectively) to conclude that the spin relaxations occur via single relaxation processes.

This change of magnetic properties is reversible, which is a result of the reversible change of the Arrhenius plot of **1**. The Δ/k_B value obtained for each condition remains almost unchanged for three drying and CH_3NO_2 addition cycles.

The structural change during drying and adsorption processes was very small, and the detail has not been elucidated. However, it can be pointed out that the easy-axis of this SCM arises from the strictly orthogonal arrangement of each easy-plane of Fe(II) ion along the chain, hence a slight deviation of the easy-plane from the ideal position might strongly affect the magnetic property of the whole chain. Moreover, neighboring Fe(II)–Fe(III) ions present a moderate antiferromagnetic interaction through a long Fe(II)–Fe(III) distance (longer than 5 Å), and during the condition change, it may be shortened with the decrease of cell parameters to enhance the magnetic interaction.

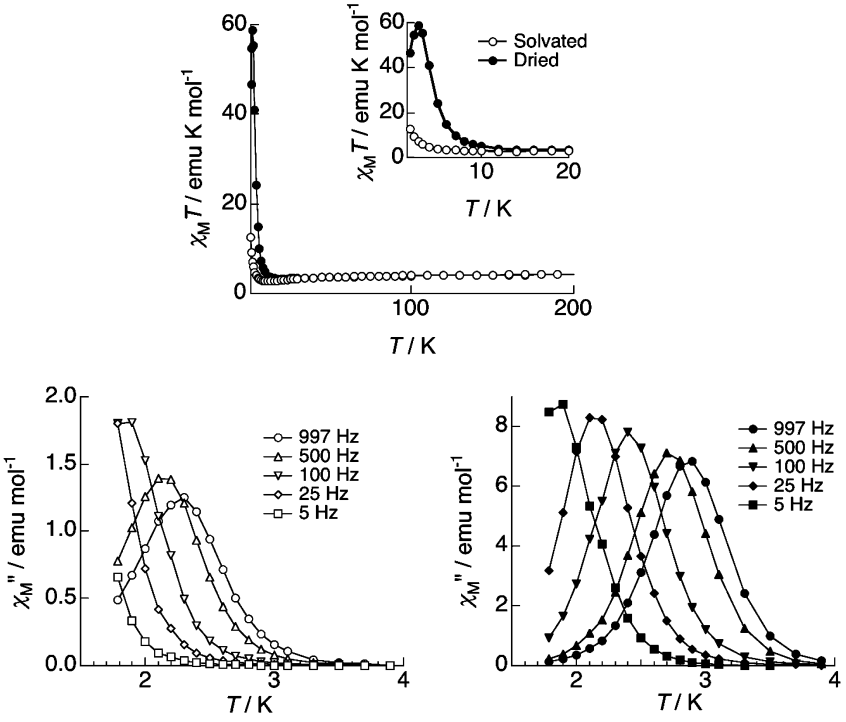

Fig. 8 (Upper) Plot of $\chi_M T$ vs. T under 0.01 T for solvated and dried samples. Solid lines are guides. (Lower) Plot of χ_M" vs. T under zero dc field for the solvated (left) and the dried (right) samples. Solid lines are guides.

SYNTHESIS AND MAGNETISM OF A DERIVATIVE OF 1

Structural changes of **1**, as described above, significantly perturb the magnetism of the twisted easy-plane system. To realize the fine-tuning of this magnetism, introduction of alkyl group(s) on the pyridyl rings of bpca$^-$ ligand in **1** would be effective from the viewpoints of structural perturbation as well as an electrochemical effect on the Fe(III) site, since the Fe(III) is directly bound to the pyridyl rings of the bpca$^-$ ligand. We have developed a synthetic procedure for derivatives of the Hbpca ligand, namely, Hbmpca [bis(4-methyl-2-pyridylcarbonyl)amine, shown in Scheme 2] and, using this new ligand, the second example of a high-spin Fe^{II} and low-spin Fe^{III} alternate SCM, *catena*-$[Fe^{II}(ClO_4)(H_2O)\{Fe^{III}(bmpca)_2\}](ClO_4)_2$ **4** was synthesized [39]. The synthetic procedure begins with the preparation of cyanopyridine from the appropriate pyridine [40,41], and the whole procedure could be readily used for similar derivatives with different alkyl, aryl, or other functional groups. The resulting cyanopyridine was heated in the presence of a catalytic amount of sodium hydride to effect trimerization, to give 1,3,5-tris(4-methyl-2-pyridyl)triazine. The triazine was reacted with an excess amount of copper nitrate to achieve hydrolysis, and the resulting mono-copper complex was treated with an ex-

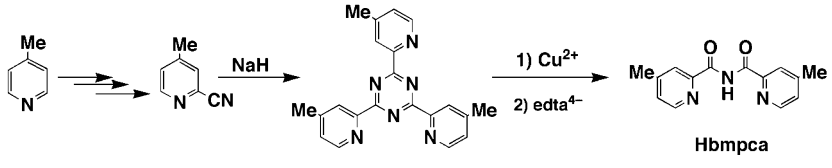

Scheme 2

cess amount of Na_4edta to obtain the free organic ligand Hbmpca. Following the methodology for **1**, the alternating Fe(II)–Fe(III) chain complex **4** was synthesized.

Black rod-like crystals were subjected to X-ray analysis (Fig. 9), which revealed that **4** comprises an alternating arrangement of $\{Fe(bmpca)_2\}^+$ units and $\{Fe(ClO_4)(H_2O)\}^+$ units to form infinite chains. High-spin Fe(II) ion in the $\{Fe^{II}(ClO_4)(H_2O)\}^+$ site is in an elongated octahedral geometry with four equatorial carbonyl oxygen atoms [2.059(3)–2.075(2) Å] and two axial oxygen atoms from one perchlorate anion and a water molecule [2.123(3)–2.154(3) Å]. The coordination environment around the Fe(II) site is similar to that of **1**, and this geometry again leads to a uniaxial zero-field splitting parameter of $D > 0$. Thus, the $S = 2$ spin on the Fe(II) ions would have a hard-axis-type anisotropy along the $O_{perchlorate}$–Fe–O_{water} axis, or easy-plane type. The shortest intra- and interchain Fe–Fe distances were estimated as 5.2161(9) Å and 10.6468(12) Å, respectively.

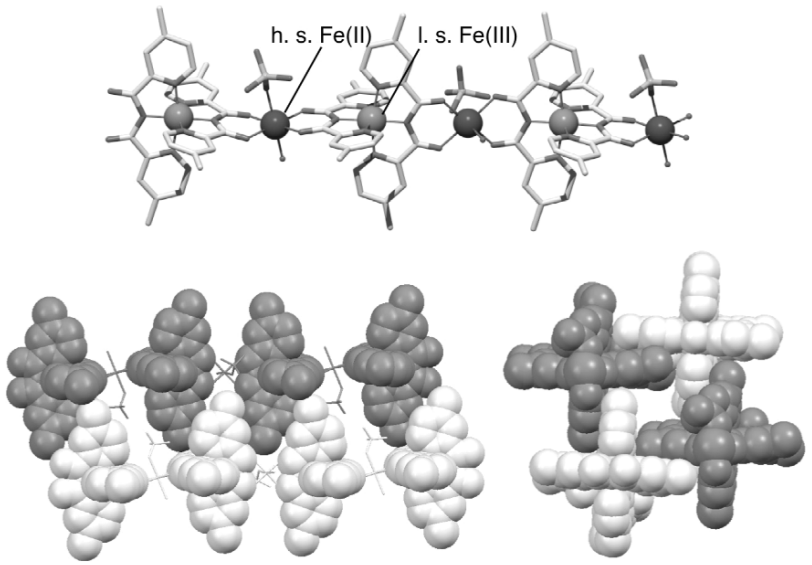

Fig. 9 (Upper) Crystal structure of the chain complex **4**. Black and gray spheres represent Fe(II) and Fe(III) ions, respectively. (Lower) Packing diagram of **4**. Each $\{Fe(bmpca)_2\}^+$ unit is depicted in a space-filling representation with deep or light gray color.

The temperature dependence of $\chi_M T$ for polycrystalline sample of **4** is clearly consistent with the presence of ferrimagnetic interactions (Fig. 10). $\chi_M T$ value takes a minimum value at 18 K (2.79 emu K mol^{-1}), which is slightly lower than that of **1** (22 K), indicating a weaker magnetic interaction between adjoining Fe(II)–Fe(III) ions than **1**. Below this temperature, $\chi_M T$ abruptly increased to a maximum value at 1.8 K (19.1 emu K mol^{-1}).

Ac magnetic susceptibility measurements were performed to observe the frequency dependence of χ_M" (Fig. 10, right). Compound **4** shows typical SCM behavior below 3 K. As the frequency was swept from 997 to 5 Hz, the temperature of maximum χ_M" shifted from 2.3 K (997 Hz) to 1.9 K (50 Hz). The temperature for the maximum χ_M" in the lower frequency fields was lower than this temperature range. Semicircle Cole–Cole plots were obtained with small α parameters (0.24–0.26), which indicates that relaxation occurs via a single process. This typical SCM behavior is again attributed to a mutually orthogonal arrangement of the Fe(II) molecular axes inducing Ising interactions along the chain observed in **1**. From an Arrhenius plot, an estimated activation energy Δ/k_B of 19(1) K was obtained. This Δ/k_B value is slightly smaller than that of **1** [27(1) K], reflecting the smaller Fe(II)–Fe(III) interaction suggested by the temperature dependence of dc susceptibility.

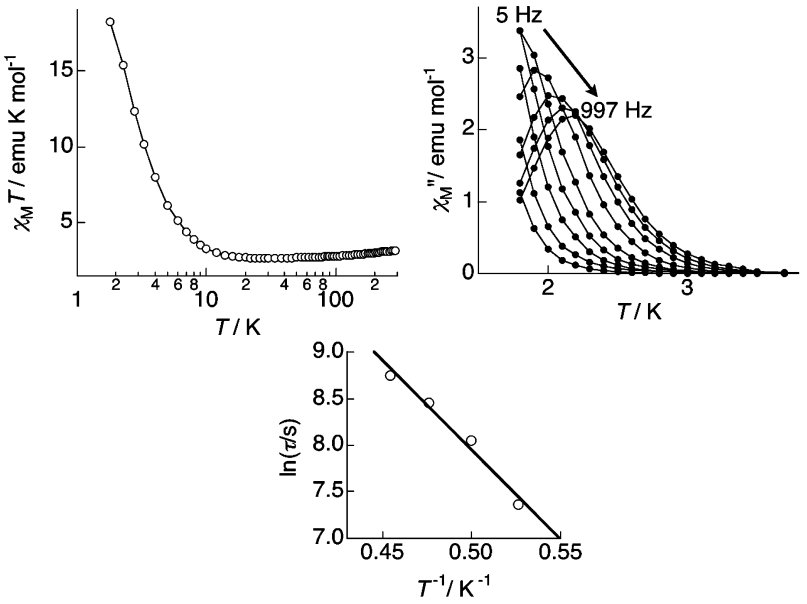

Fig. 10 (Left) Temperature dependence of $\chi_M T$ for **2**. (Right) Temperature dependence of χ_M". (Bottom) Arrhenius plot.

CONCLUSION

In conclusion, alternating Fe(II) (high-spin)–Fe(III) (low-spin) mixed-valence SCMs were synthesized by the bottom-up approach using the mononuclear complexes as a ligand. These twisting easy-plane systems are unique in that they display easy-axis anisotropy over the whole chain, which gives rise to slow magnetization reversal, despite possessing Fe(II) ions with easy-plane single-ion anisotropy. Since the easy-axis anisotropy of these SCMs arises from the spatial arrangement of the hard axis of the Fe(II) ions, the magnetism of **1** is very sensitive to a small structural change such as a magnetic sponge, and **1** is the first example of an SCM which shows the solvent-induced reversible change of magnetic properties.

REFERENCES

1. L. Thomas, F. Lionti, R. Ballou, D. Gatteschi, R. Sessoli, B. Barbara. *Nature* **383**, 145 (1996).
2. D. Gatteschi, R. Sessoli. *Angew. Chem., Int. Ed.* **42**, 268 (2003).
3. W. Wernsdorfer, R. Sessoli. *Science* **284**, 133 (1999).
4. S. M. J. Aubin, Z. Sun, L. Pardi, J. Krzystek, K. Folting, L.-C. Brunel, A. L. Rheingold, G. Christou, D. N. Hendrickson. *Inorg. Chem.* **38**, 5329 (1999).
5. E.-C. Yang, D. N. Hendrickson, W. Wernsdorfer, M. Nakano, L. N. Zakharov, R. D. Sommer, A. L. Rheingold, M. Ledezma-Gairaud, G. Christou. *J. Appl. Phys.* **91**, 7382 (2002).
6. V. Chandrasekhar, B. M. Pandian, R. Azhakar, J. J. Vittal, R. Clérac. *Inorg. Chem.* **46**, 5140 (2007).
7. S. Osa, T. Kido, N. Matsumoto, N. Re, A. Pochaba, J. Mrozinski. *J. Am. Chem. Soc.* **126**, 420 (2004).
8. C. Aronica, G. Pilet, G. Chastanet, W. Wernsdorfer, J.-F. Jacquot, D. Luneau. *Angew. Chem., Int. Ed.* **45**, 4659 (2006).

9. A. Caneschi, D. Gatteschi, N. Lalioti, C. Sangregorio, R. Sessoli, G. Venturi, A. Vindigni, A. Rettori, M. G. Pini, M. A. Novak. *Angew. Chem., Int. Ed.* **40**, 1760 (2001).
10. R. Clérac, H. Miyasaka, M. Yamashita, C. Coulon. *J. Am. Chem. Soc.* **124**, 12837 (2002).
11. R. Lescouëzec, J. Vaissermann, C. Ruiz-Pérez, F. Lloret, R. Carrasco, M. Julve, M. Verdaguer, Y. Dromzee, D. Gatteschi, W. Wernsdorfer. *Angew. Chem., Int. Ed.* **42**, 1483 (2003).
12. L. Bogani, C. Sangregorio, S. Sessoli, D. Gatteschi. *Angew. Chem., Int. Ed.* **44**, 5817 (2005).
13. H. Oshio, N. Hoshino, T. Ito. *J. Am. Chem. Soc.* **122**, 12602 (2000).
14. H. Oshio, N. Hoshino, T. Ito, M. Nakano. *J. Am. Chem. Soc*. **126**, 8805 (2004).
15. H. Oshio, M. Nakano. *Chem.—Eur. J.* **11**, 5178 (2005).
16. T. Kajiwara, M. Nakano, Y. Kaneko, S. Takaishi, T. Ito, M. Yamashita, A. Igashira-Kamiyama, H. Nojiri, Y. Ono, N. Kojima. *J. Am. Chem. Soc.* **127**, 10150 (2005).
17. A. Kamiyama, T. Noguchi, T. Kajiwara, T. Ito. *Angew. Chem., Int. Ed.* **39**, 3130 (2000).
18. A. Kamiyama, T. Noguchi, T. Kajiwara, T. Ito. *Inorg. Chem.* **41**, 507 (2002).
19. A. Kamiyama, T. Noguchi, T. Kajiwara, T. Ito. *Cryst. Eng. Commun.* **5**, 231 (2003).
20. T. Kajiwara, R. Sensui, T. Noguchi, A. Kamiyama, T. Ito. *Inorg. Chim. Acta* **337**, 299 (2002).
21. T. Kajiwara, T. Ito. *Mol. Cryst. Liq. Cryst.* **335**, 73 (1999).
22. K. S. Cole, R. H. Cole. *J. Chem. Phys.* **9**, 341 (1941).
23. C. J. F. Boettcher. *Theory of Electric Polarization*, Elsevier, Amsterdam (1952).
24. R. J. Glauber. *J. Math. Phys.* **4**, 294 (1963).
25. C. Coulon, R. Clérac, L. Lecren, W. Wernsdorfer, H. Miyasaka. *Phys. Rev*. *B* **69**, 132408 (2004).
26. T. Kajiwara, I. Watanabe, Y. Kaneko, S. Takaishi, M. Enomoto, N. Kojima, M. Yamashita. *J. Am. Chem. Soc.* **129**, 12360 (2007).
27. S. J. Blundell, F. L. Pratt, T. Lancaster, I. M. Marshall, C. A Steer, W. Hayes, T. Sugano, J.-F. Letard, A. Caneschi, D. Gatteschi, S. L. Heath. *Physica B* **326**, 556 (2003).
28. K. Takeda, K. Awaga, S. Ohira, I. Watanabe. *Synth. Met.* **133**–**134**, 609 (2003).
29. A. Lascialfari, D. Gatteschi, F. Borsa, A. Shastri, Z. H. Jang, P. Carretta. *Phys. Rev. B* **57**, 514 (1998).
30. S. J. Blundell. *Chem. Rev.* **104**, 5717 (2004).
31. I. Watanabe, M. Aoyama, M. Akoshima, T. Kawamata, T. Adachi, Y. Koike, S. Ohira, W. Higemoto, K. Nagamine. *Phys. Rev. B* **62**, R11985 (2000).
32. Y. J. Uemura, T. Yamazaki, D. R. Harshman, M. Senba, E. J. Ansaldo. *Phys. Rev. B* **31**, 546 (1985).
33. S.-i. Ohkoshi, S. Yorozu, O. Sato, T. Iyoda, A. Fujushima, K. Hashimoto. *Appl. Phys. Lett.* **70**, 1040 (1997).
34. L. Egan, K. Kamenev, D. Papanikolaou, Y. Takabayashi, S. Margadonna. *J. Am. Chem. Soc.* **128**, 6034 (2006).
35. S.-i. Ohkoshi, K.-i. Arai, Y. Sato, K. Hashimoto. *Nat. Mater.* **3**, 857 (2004).
36. O. Kahn, J. Larionova, J. V. Yakhmi. *Chem.—Eur. J.* **5**, 3443 (1999).
37. D. Maspoch, D. Ruiz-Molina, K. Wurst, N. Domingo, M. Cavallini, F. Biscarini, J. Tejada, C. Rovira, J. Veciana. *Nat. Mater.* **2**, 190 (2003).
38. Y. Kaneko, T. Kajiwara, H. Yamane, M. Yamashita. *Polyhedron* **26**, 2074 (2007).
39. H. Tanaka, T. Kajiwara, Y. Kaneko, S. Takaishi, M. Yamashita. *Polyhedron* **26**, 2105 (2007).
40. F. H. Case, E. Koft. *J. Am. Chem. Soc.* **81**, 905 (1959).
41. R. T. Shuman, P. L. Ornstein, J. W. Paschal, P. D. Gesellchen. *J. Org. Chem*. **55**, 738 (1990).